Topology-Preserving Hard Pixel Mining for Tubular Structure Segmentation - Supplementary Material

BMVC 2023 Submission # 846

1 Persistent Homology-based HPM

1.1 Persistent Homology on Image

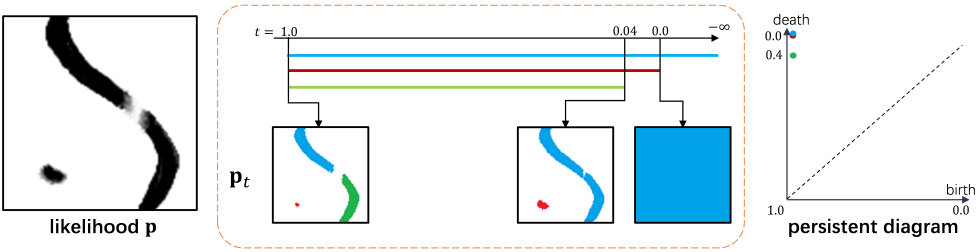

Figure 1: Illustration of persistent homology on image. Left figure is a likelihood map $\mathbf{p}$. The Middle bottom one shows the binarized maps of $\mathbf{p}$ with different thresholds. As the threshold t deceasing, the foreground of current snapshot is covered by the counterpart of the next moment. Here we only consider 0-dimensional features, which refer to connected components and are masked in different colors. The middle top persistent bars in different colors correspond to the lifetime of different topological features. The start and end t of these bars form the points of the right persistent diagram.

In the context of segmentation models, the output $\mathbf{p}$ is a likelihood matrix. Binarization need to be performed to obtain the predicted label. Given the probability threshold t, binarized prediction $\mathbf{p}_t$ has the same shape with $\mathbf{p}$, where for each pair (p_t, p) that taken from the same position of $\mathbf{p}_t$ and $\mathbf{p}$ we have:

$$p_t = \begin{cases} 1, & p >= t; \\ 0, & \text{otherwise}. \end{cases} \tag{1}$$

We use f^t to denote the foreground of $\mathbf{p}_t$. Obviously, the value of t influences the resulting pattern f_t, thereby affecting its topological structures that refers to connected components for 0-dimension and holes for 1-dimension [3, 4]. As illustrated in Fig. 1, persistent homology captures all topological structures through a filtration $\mathcal{F}$, which is a monotonically growing sequence generated by progressively decreasing the threshold t:

$$\mathcal{F} = \left[f^{t_1}, f^{t_2}, \cdots, f^{t_n}\right], \; t_1 > t_2 > \cdots > t_n; \tag{2}$$

and we have:

$$f^{t_1} \subseteq f^{t_2} \subseteq \cdots \subseteq f^{t_n}. \tag{3}$$

During this process, some new topological structures emerge while existing ones are killed. The thresholds corresponding to the birth and death of a topological structure constitute a point in the persistent diagram that can be calculated efficiently through cubical complex [1, 8, 10]. Each birth or death occurs at a specific pixel. This kind of pixels are called critical points and they introduce topological changes.

1.2 Topology-Preserving Cost Function by Hu et al. [6]

Hu et al. [6] propose a topology-preserving cost function based on persistent homology. They calculate the persistent diagrams $\mathrm{Dgm}(\mathbf{p})$ and $\mathrm{Dgm}(\mathbf{y})$ for prediction $\mathbf{p}$ and ground-truth $\mathbf{y}$, respectively. Note that all points from $\mathrm{Dgm}(\mathbf{y})$ have the same coordinate $(1,0)$. A distance-based matching algorithm [7] is further performed to establish correspondences between the points in these two diagrams. The unmatched points in $\mathrm{Dgm}(\mathbf{p})$ are considered as noise and projected onto the diagonal line. As we mentioned before, every point in persistent diagram consists of the birth and death threshold of a topological feature, and therefore corresponds two critical points. For a given point $d_\mathbf{p} \in \mathrm{Dgm}(\mathbf{p})$ and its critical points $(c_{\mathrm{birth}}, c_{\mathrm{death}})$, if $d_\mathbf{p}$ is successfully matched to a point $d_\mathbf{y} \in \mathrm{Dgm}(\mathbf{y})$, the loss to align $d_\mathbf{p}$ and $d_\mathbf{y}$ can be formulated as:

$$l_{\mathrm{Dgm}}(d_\mathbf{p}) = (1.0 - c_{\mathrm{birth}})^2 + c_{\mathrm{death}}^2. \tag{4}$$

Otherwise, $d_\mathbf{p} \in \mathrm{Dgm}(\mathbf{p})$ is projected to the diagonal by:

$$l_{\mathrm{Dgm}}(d_\mathbf{p}) = (c_{\mathrm{death}} - c_{\mathrm{birth}})^2. \tag{5}$$

The overall cost function is calculated as following:

$$\mathcal{L}_{\mathrm{Dgm}} = \sum_{d_\mathbf{p} \in \mathrm{Dgm}(\mathbf{p})} l_{\mathrm{Dgm}}(d_\mathbf{p}). \tag{6}$$

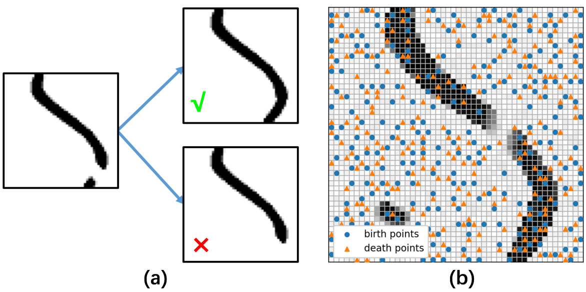

Figure 2: Drawbacks of Hu et al. [6]. (a) Aligning two persistent diagram can leads to geometrically incorrectness. (b) The topology of a likelihood map can be very complicated. Subtle variation of pixel values result in a large number of trivial critical points.

1.3 Persistent Homology-based HPM

Hu et al. [6] has two noticeable drawbacks. Firstly, aligning the persistent diagrams is not sufficient from a geometric perspective. Fig. 2(a) shows that minimizing $\mathcal{L}_{\text{Dgm}}$ leads to two possible results. Both of them have the correct topology, while the top one are geometrically incorrect. Secondly, the topology of a likelihood map could be very complicated, resulting in a large number of critical points as show in Fig. 2(b). Therefore, according to the authors, the matching process can be quite difficult for large image patches. Also, most of critical points are introduced by slight difference among pixels and are actually trivial and even harmful for topology preservation. In their experiment, the patch size is limited to (65×65) to get reasonable results.

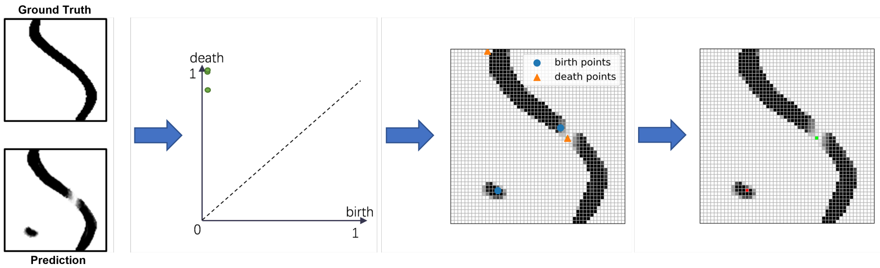

Figure 3: Illustration of persistent homology-based HPM: cubical complex of prediction is calculated to generate a set of critical points, each of which corresponds to the birth or death of a topological structure. Mis-segmented critical points are marked as hard pixels.

The persistent homology-based HPM (PHPM) is an improved version of Hu et al. [6]. Instead of directly matching and aligning the critical points like Hu et al. [6], we use critical points to mine hard pixels. A pre-processing is performed before the computation of persistent homology, so that the topology analysis can pay most attention on mis-segmented pixels. PHPM can be formulated as follows:

$$H_{\text{p}} = \bigcup_{d \in D} C_d\left(f\left(\mathbf{p}, \mathbf{y}, t\right)\right). \tag{7}$$

The set D encompasses the dimensions of topological features that hold our interest, $C_d(\cdot)$ denotes the function to get the d-dim critical points of input image, f is the pre-processing function that increases the intensity of all true positive pixels to 1.0 and all true negative pixels to 0.0. It returns a matrix $\mathbf{p}_f$ with the same shape as input $\mathbf{p}$ and $\mathbf{y}$. For each quadruplet (p_f, p_t, p, y) that consists of elements taken from the same position of $\mathbf{p}_f$, $\mathbf{p}_t$, $\mathbf{p}$ and $\mathbf{y}$, we have:

$$p_f = \begin{cases} p, & \text{if } p_t \neq y; \\ y, & \text{otherwise.} \end{cases} \tag{8}$$

Fig. 3 gives an illustration of PHPM. Training with PHPM leads to correct topology and geometry. Also, the pre-process significantly reduce the number of trivial topological features. So PHPM can be applied on larger image patches and demonstrates a higher topology-preserving ability comparing to [6].

1.4 Expremental Results

Table. 1 quantitatively evaluate the performance of models training with different loss functions on 6 public datasets [2, 5, 9, 11]. The size of image patches is 256 × 256 for 2D data and 128 × 128 × 72 for 3D data. Comparing to Hu et al. [6], training with PHPM achieve higher scores for all metrics, especially for topology-aware metrics, which means that PHPM is more advanced version of [6] and demonstrates a better topological preservation capability.

Table 1: Quantitative experimental results.

Dataset	Method	Dice	mIoU	VOI	ARE	β-0 Error	β-1 Error
CREMI-A	U-Net + Hu et al.	**0.9134**	**0.8407**	0.4002	0.2332	2.296	24.752
	U-Net + PHPM	0.9133	0.8405	**0.3819**	**0.2060**	**2.112**	**20.352**
CREMI-B	U-Net + Hu et al.	0.8538	0.7497	1.1434	0.6199	18.128	64.064
	U-Net + PHPM	**0.8540**	**0.7502**	**1.0444**	**0.5724**	**15.672**	**56.056**
CREMI-C	U-Net + Hu et al.	**0.8937**	**0.8083**	0.6974	0.3678	6.878	47.496
	U-Net + PHPM	0.8934	0.8077	**0.6383**	**0.3243**	**5.772**	**39.089**
ISBI12	U-Net + Hu et al.	0.8313	0.7122	0.6869	0.1555	**2.967**	7.933
	U-Net + PHPM	**0.8313**	**0.7123**	**0.6805**	**0.1400**	3.200	**7.583**
Roads	U-Net + Hu et al.	0.7237	0.5755	0.7605	0.3470	10.492	29.820
	U-Net + PHPM	**0.7295**	**0.5823**	**0.7339**	**0.3372**	**8.826**	**29.232**
ICAS-d (3D)	U-Net + Hu et al.	-	-	-	-	-	-
	U-Net + PHPM	**0.6059**	**0.4407**	**0.0091**	**0.0012**	**4.590**	**0.000**

References

[1] Madjid Allili, Konstantin Mischaikow, and Allen Tannenbaum. Cubical homology and the topological classification of 2d and 3d imagery. In *Proceedings 2001 international conference on image processing (Cat. No. 01CH37205)*, volume 2, pages 173–176. IEEE, 2001.

[2] Ignacio Arganda-Carreras, Srinivas C Turaga, Daniel R Berger, Dan Cireşan, Alessandro Giusti, Luca M Gambardella, Jürgen Schmidhuber, Dmitry Laptev, Sarvesh Dwivedi, Joachim M Buhmann, et al. Crowdsourcing the creation of image segmentation algorithms for connectomics. *Frontiers in neuroanatomy*, 9:142, 2015.

[3] Tamal Krishna Dey and Yusu Wang. *Computational topology for data analysis*. Cambridge University Press, 2022.

[4] Herbert Edelsbrunner, David Letscher, and Afra Zomorodian. Topological persistence and simplification. In *Proceedings 41st annual symposium on foundations of computer science*, pages 454–463. IEEE, 2000.

[5] Jan Funke, Fabian Tschopp, William Grisaitis, Arlo Sheridan, Chandan Singh, Stephan Saalfeld, and Srinivas C Turaga. Large scale image segmentation with structured loss based deep learning for connectome reconstruction. *IEEE transactions on pattern analysis and machine intelligence*, 41(7):1669–1680, 2018.

[6] Xiaoling Hu, Fuxin Li, Dimitris Samaras, and Chao Chen. Topology-preserving deep image segmentation. *Advances in neural information processing systems*, 32, 2019.

[7] Michael Kerber, Dmitriy Morozov, and Arnur Nigmetov. Geometry helps to compare persistence diagrams, 2017.

[8] Clément Maria, Jean-Daniel Boissonnat, Marc Glisse, and Mariette Yvinec. The gudhi library: Simplicial complexes and persistent homology. In *Mathematical Software–ICMS 2014: 4th International Congress, Seoul, South Korea, August 5-9, 2014. Proceedings 4*, pages 167–174. Springer, 2014.

[9] Volodymyr Mnih. *Machine learning for aerial image labeling*. University of Toronto (Canada), 2013.

[10] Hubert Wagner, Chao Chen, and Erald Vuçini. Efficient computation of persistent homology for cubical data. In *Topological methods in data analysis and visualization II: theory, algorithms, and applications*, pages 91–106. Springer, 2011.

[11] An Zeng, Chunbiao Wu, Meiping Huang, Jian Zhuang, Shanshan Bi, Dan Pan, Najeeb Ullah, Kaleem Nawaz Khan, Tianchen Wang, Yiyu Shi, et al. Imagecas: A large-scale dataset and benchmark for coronary artery segmentation based on computed tomography angiography images. *arXiv preprint arXiv:2211.01607*, 2022.